Adaptive Beamforming Using Steering Vector Correction for Phased-Array Weather Radar

Hiroshi Kikuchi ⓘ, *Member, IEEE*, Eiichi Yoshikawa ⓘ, *Member, IEEE*, Tomoo Ushio, *Member, IEEE*, and Yasuhide Hobara

Abstract—In December 2017, a dual-polarized (DP) phased-array weather radar (PAWR) was deployed to observe precipitation in Tokyo, Japan. The DP-PAWR has the following characteristics: high-temporal-resolution observations for a volume scan of 30 s in a 60 km range, high-density observations below a 15 km altitude, improved rain rate estimation using dual-polarimetric observations, and hydrometer classification abilities. To achieve high-temporal-resolution observations, wide transmitted waves with a beam width up to 5° are used for elevation angles. Although Fourier-domain digital beamforming can be used for receiving waves, the high sidelobe level of the antenna pattern using this type of beamforming results in substantial errors (e.g., overestimation of received power) because of ground clutter echoes. To solve this problem, an adaptive beamforming method based on the minimum mean square error (MMSE) was developed for a single-polarization phased-array radar. In this study, signal processing procedures, including the steering vector correction of real measurement data, are developed to apply the MMSE method to the DP-PAWR. The effect of phase errors and ground clutter on the dual-polarimetric parameters is evaluated via numerical simulations. Subsequently, the proposed method is applied to real measurement data of the DP-PAWR. Consequently, it is found that the clutter suppression achieved using the proposed method is clearly superior to that achieved using Fourier-domain digital beamforming.

Index Terms—Adaptive signal processing, phased-array radar, polarimetric radar observations, remote sensing.

I. INTRODUCTION

PHASED-ARRAY radar systems with improved temporal resolution are being developed worldwide for precipitation measurement [1]–[9]. In Japan, four single-polarization (SP) phased-array weather radars (PAWRs) have been operating in the cities of Osaka, Kobe, Okinawa, and Tsukuba, since 2012 [10], [11]. The SP-PAWRs, jointly developed by Osaka University, the National Institute of Information and Communications Technology, and Toshiba Infrastructure Systems & Solutions, allow

high-density observations below 15-km altitude. The obtained high-temporal-resolution and high-density observations help to clearly evaluate severe phenomena such as microdownbursts within a thunderstorm in three dimensions [12]. Consequently, the data provided by the SP-PAWRs enable short-term weather forecasting.

As a successor to the SP-PAWR, the dual-polarized (DP) PAWR was jointly developed by the original SP-PAWR developers, Nagoya University, and Tokyo Metropolitan University, in December 2017. The DP-PAWR is also known as the multiparameter PAWR, in Japan, and its current observation area is the Kanto area, including the urban area in Tokyo. In addition to the advantages of the original PAWR, the DP-PAWR can improve the accuracy of rainfall estimation and hydrometer classification ability using dual (horizontal and vertical) polarization observations [13]–[17].

In both the DP-PAWR and SP-PAWR, the antenna can rotate with respect to the azimuth dimension. On the other hand, in terms of elevation dimension, electronic scanning is performed via digital beamforming. The transmitted wave of the DP-PAWR is a fan beam with widths of 1.2° and 5° for azimuth and elevation, respectively. For the received waves, digital beamforming improves the resolution of the elevation dimension to 0.8°. In the DP-PAWR, Fourier-domain beamforming (FR) is adopted for digital beamforming. However, the high sidelobe level of the antenna pattern obtained using FR causes the received power to be overestimated because of ground clutter echoes. In the case of the DP-PAWR, ground clutter echoes occur because of tall buildings in the Tokyo area. To solve this problem, an adaptive beamforming method based on the minimum mean square error (MMSE) has been proposed for the SP-PAWR, which also operates in urban areas [18]. The MMSE-based beamforming method effectively suppresses sidelobes and handles real measurement data of the SP-PAWR. For MMSE-based beamforming, the power received by each antenna element is assumed to be the same when using the SP-PAWR. Although the SP-PAWR consists of a two-dimensional (2-D) array antenna, the received signals from the antenna elements arranged horizontally are summed uniformly. The signals received by each row of antenna elements are the same because the number of horizontal elements is constant. Consequently, the SP-PAWR shows behavior similar to a 1-D phased-array antenna arranged vertically, where digital beamforming is applied only in the elevation domain. In contrast, the received power of the DP-PAWR differs for each

Hiroshi Kikuchi and Yasuhide Hobara are with The University of Electro-Communications, Tokyo 182-8585, Japan (e-mail: hkikuchi@uec.ac.jp; hobara@ee.uec.ac.jp).

Eiichi Yoshikawa is with the Japan Aerospace Exploration Agency, Tokyo 181-0015, Japan (e-mail: yoshikawa.eiichi@jaxa.jp).

Tomoo Ushio is with the Osaka University, Osaka 565-0871, Japan (e-mail: ushio@eei.eng.osaka-u.ac.jp).
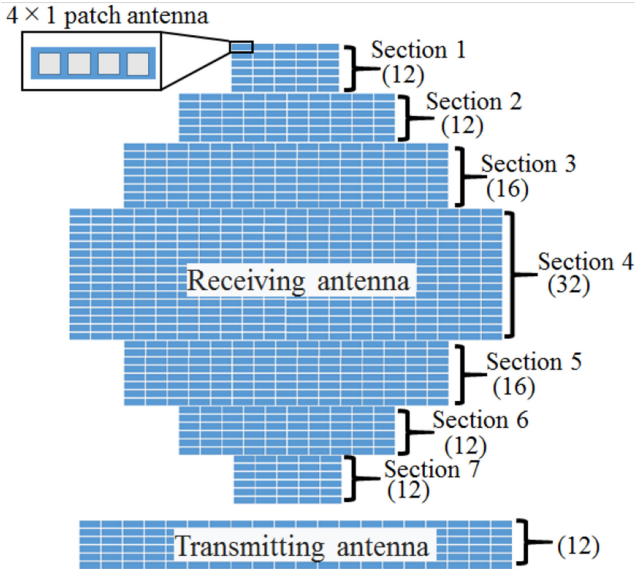
Fig. 1. Antenna shapes in DP-PAWR. The number of antenna elements is given in parenthesis.

row of antenna elements in the vertical direction because the number of horizontal elements is different. When MMSE-based beamforming is employed, steering vector errors occur in the amplitude of the DP-PAWR.

The remainder of this article is organized as follows. In Section II, we extend the MMSE-based method by adding steering vector correction for the DP-PAWR using real measurement data. In Section III, the evaluation of effects of phase errors and ground clutter on dual-polarimetric parameters via numerical simulations are discussed. In Section IV, the application of the proposed extension of MMSE-based beamforming to the real measurement data of the DP-PAWR is considered. The conclusions are presented in Section V.

II. METHODOLOGY

A. Antenna Shape and Signal Tapering of DP-PAWR

Fig. 1 shows the shapes of the receiving and transmitting antennas of the DP-PAWR. Each panel is comprised of four patch antennas, represented by the box in the top left corner. As the signals of the transmitting and receiving antennas are integrated along the horizontal direction, the patch antennas arranged horizontally function as a subarray. Consequently, the receiving antenna has 112 vertical subarrays (from top to bottom, subarrays 1–112), and the transmitting antenna has 12 subarrays and conforms to a linear array antenna. Electronic scanning is performed via digital beamforming in the elevation dimension. The transmitting antenna has the same number of patch antennas along the horizontal direction. Given that the signals are integrated, the beam width formed along the azimuth dimension is 1.2°.

As shown in Fig. 1, the receiving antenna has different numbers of patch antennas along the horizontal direction. This

antenna can be divided into seven sections from top to bottom, as shown in Fig. 1. Sections 1 (subarrays 1–12) and 7 (subarrays 101–112), sections 2 (subarrays 13–24) and 6 (subarrays 89–100), and sections 3 (elements 25–40) and 5 (subarrays 73–88) have 20, 40, and 60 patch antennas along the horizontal direction, respectively. Section 4 (subarrays 41–72) has the largest number of patch antennas (80) along the horizontal direction. The total number of patch antennas for the receiving and transmitting antennas are 5920 and 960, respectively. The vertical subarray spacing is 16.5 mm. Thus, 112 in-phase/quadrature (I/Q) signals are obtained and stored in the receiving unit. After the recording, pulse compression processing and digital beamforming are performed on the received signals.

B. FR Beamforming

We assume that a phased array consists of a linear array antenna with N elements, which can be rephrased as subarrays in the DP-PAWR case. The observation equation is expressed as a discrete time series as follows:

$$\mathbf{x}_l = \mathbf{A}\mathbf{y}_l + \boldsymbol{v}_l \tag{1}$$

$$\mathbf{x}_l = [\, x_{l,0} \; x_{l,1} \; \ldots \; x_{l,N-1} \,]^{\mathrm{T}} \tag{2}$$

$$\mathbf{y}_l = [\, y_{l,0} \; y_{l,1} \; \ldots \; y_{l,M-1} \,]^{\mathrm{T}} \tag{3}$$

$$\mathbf{A} = [\, a(\theta_0) \; a(\theta_1) \; \ldots \; a(\theta_{M-1}) \,] \tag{4}$$

where $\mathbf{x}_l$ is the vector of complex amplitudes of the lth received time sample, l is an index of transmitted pulses, $\mathbf{y}_l$ is the M-dimensional vector of complex amplitudes associated with M precipitation profiles at different elevation angles for an arbitrary range bin, $\mathbf{A}$ is the matrix of steering vectors, $\boldsymbol{v}_l$ is the additive white Gaussian noise vector, and T is the transpose operator.

The steering vector depends on the incidence angle θ that corresponds to the elevation angle in the DP-PAWR, which is expressed as follows:

$$\boldsymbol{a} = [\exp(-j\omega_0) \; \exp(-j\omega_1) \; \ldots \; \exp(-j\omega_{N-1}) \,]^{\mathrm{T}} \tag{5}$$

with

$$\omega_n(\theta) = 2\pi/\lambda \; (dn\sin\theta) \tag{6}$$

where λ is the wavelength of the transmitted wave, and d is the spacing between neighboring antenna elements.

To improve the sidelobe properties, in this study, the Hann window is used in the FR method. The following equation generates the coefficients of a Hann window:

$$win(n) = 0.5 \left(1 - \cos 2\pi \frac{n}{N}\right), \text{ if } 0 \leq \frac{n}{N} \leq 1. \tag{7}$$

Considering the window function, $\mathbf{x}_l$ can be rewritten using the following:

$$\mathbf{x}'_l == [\, win(1)\,x_{l,0} \; win(2)\,x_{l,0}x_{l,1} \; \ldots \; win(N)\,x_{l,N-1} \,]^{\mathrm{T}}. \tag{8}$$

Beamformer output $\boldsymbol{B}$ can be obtained as follows:

$$\boldsymbol{B} = \mathbf{w}^H \mathbf{x}'_l \tag{9}$$

$$\boldsymbol{B} = [\, b_{l,0} \; b_{l,1} \; \ldots \; b_{l,M-1} \,]^{\mathrm{T}} \tag{10}$$

where $\mathbf{w}$ is the complex weighting vector for the received complex amplitudes of each antenna element, and H denotes the Hermitian transpose. M is the number of particular elevation angles ranging from $0°$ to $90°$.

FR beamforming is the most basic digital beamforming method whose weighting vector, expressed as

$$\boldsymbol{w}_{\mathrm{FR}} = \boldsymbol{a}\left(\theta\right)/N \tag{11}$$

is proportional to the steering vector acting on the phase of signals received at each element.

C. MMSE-Based Beamforming

MMSE-based beamforming is proposed using an adaptive gain-constrained pulse compression algorithm [19]–[21]. The MMSE-based beamforming method is used for the SP-PAWR, and various numerical simulations have been conducted accordingly [18]. The weighting vector of MMSE-based beamforming is expressed as follows:

$$\boldsymbol{w}_{\mathrm{MMSE}} = \frac{\boldsymbol{R}^{-1}\boldsymbol{a}\left(\theta\right)}{\boldsymbol{a}^{\mathrm{H}}\left(\theta\right)\boldsymbol{R}^{-1}\boldsymbol{a}\left(\theta\right)} \tag{12}$$

with

$$\boldsymbol{R} = \boldsymbol{A}\boldsymbol{R}_y\boldsymbol{A}^{\mathrm{H}} + \boldsymbol{R}_n \tag{13}$$

where $\boldsymbol{R}_y$ and $\boldsymbol{R}_n$ are the covariance matrices of $\mathbf{y}_l$ and an additive noise, such as a thermal noise, respectively. The additive noise is assumed to be white, and $\mathbf{y}_l$ is an unknown vector. The MMSE weight is calculated iteratively using a priori information (i.e., FR solution). The iterations to obtain the MMSE solution continue until the normalized root-mean-square error (RMSE) between the current and previous solutions (i.e., array output powers) is below a threshold, which we set to -30 dB by referring to the value used in [18]. The MMSE is a suitable metric to measure precipitation using the SP-PAWR with this threshold, and therefore an optimal solution can be obtained iteratively [18].

D. MMSE-Based Beamforming With Corrected Steering Vector

While FR beamforming uses only phase information, MMSE-based beamforming adjusts the amplitude and phase information of each element to determine optimal weights. In adaptive beamforming, the amplitude information of a steering vector should be estimated according to the received signal. We propose MMSE-based beamforming that resolves the amplitude bias error because of the difference of the number of receiving patch antennas.

When the receiving power has a bias error, the steering vector expressed in (5) is resolved by adding an amplitude correction coefficient C as follows:

$$\boldsymbol{a}' = [C_0\exp\left(-j\omega_0\right)\ C_1\exp\left(-j\omega_1\right)$$
$$\dots\ C_{N-1}\exp\left(-j\omega_{N-1}\right)]^{\mathrm{T}}. \tag{14}$$

Thus, an optimal amplitude correction coefficient of each subarray is required. As the DP-PAWR has different numbers
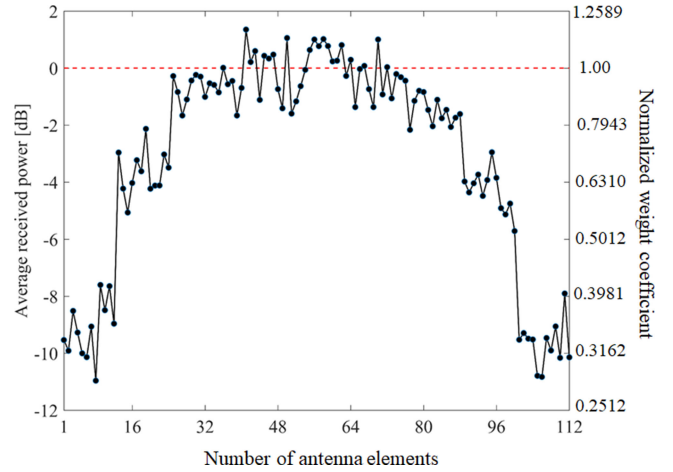

Fig. 2.   Average received power of antenna elements of DP-PAWR.

of patch antennas arranged along the horizontal direction (see Fig. 1), the amplitude of the received signal should be considered. The analytical estimation of the value of C of each subarray is difficult because the observed data include attenuation during signal processing and attenuation due to various hardware such as cable loss.

To estimate the optimal values of C, the received powers of each subarray are compared using the actual ground clutter data obtained using the DP-PAWR on a sunny day. In this case, 47 736 clutter data points (e.g., 702 positions $\times$ 68 pulses = 47 736 points) are used. Data points reflected from the clutter (e.g., buildings) with respect to the antenna are received as plane waves with respect to the antenna surface. Hence, a fixed power value is assumed to be received by each subarray. Fig. 2 shows the average power received by the subarray of the DP-PAWR. The left and right vertical axes represent the normalized received power and weight coefficient (C). Data are divided into four levels with the same number of patch antennas. Assuming that the received radio wave is a plane wave, the received power of sections 1 (1–12) and 7 (101–112) should be the same. Similarly, the powers of sections 2 (13–24) and 6 (89–100), sections 3 (25–40) and 5 (73–88), and section 4 (41–72) are obtained from the observed data. In this figure, the differential received powers based on the mean values of the received powers in section 4 are shown (left vertical axis). The average values in decibels are converted into magnitude measurements (right vertical axis). The value of C of each subarray is then estimated as the average of the received power of the subarray, as shown in Fig. 2.

The calibration of the dual polarization radar variables poses a significant issue with regard to dual polarization phased arrays. In this method, the same weight vector must be used for both the horizontal and vertical signals. The horizontal (copolar) and vertical (cross polar) antenna patterns should also have the same main-beam shape. Furthermore, it is important that the antenna characteristics match, whereby a highly accurate polarimetric measurement is ensured. The calibration method of the dual polarization radar valuables is implemented using the real measurement data as shown in previous studies (e.g., [26]).

In Section III-A, we describe the effectiveness of the proposed MMSE-based beamforming with steering vector correction (scMMSE) via numerical simulations. In addition, we report the effect of phase error on polarization parameters, which must be considered when applying beamforming to the actual observation data.

III. NUMERICAL SIMULATIONS

A. Effectiveness of Steering Vector Correction

The effectiveness of the proposed scMMSE beamforming was evaluated via numerical simulations using received signals, considering point and distributed targets. The simulations were based on the specifications of the DP-PAWR. The frequencies of the transmitting waves and pulse repetitions were 9.4 GHz and 20 kHz, respectively. The number of transmitting pulses was 68. The time series of the received signals were generated by the following procedure described in [16]. These signals exhibited the characteristic of a Gaussian spectral distribution and randomness [17]. Fig. 3(a) and (b) show the simulation results for point and distributed targets, respectively. In Fig. 3(a), two point targets, such as an airplane and ground clutter, receive a power of -70 and -44 dBm at $20°$ and $30°$ elevation angles, respectively. The results of FR are overestimated around the target (18–$22°$ and 27–$33°$). The results of MMSE-based beamforming without steering vector correction (MMSE) are not accurate for both targets. In fact, either the estimation peaks are shifted or several peaks are determined around elevation angles of $20°$ and $30°$. In contrast, the proposed scMMSE estimation is accurate. The two targets are clearly detected, with the peaks of these targets receiving a power of -70 and -43 dBm. The proposed scMMSE shows a slight overestimation because of the integration of the main beam; however, this effect occurs in every beamforming method. Fig. 3(b) shows the estimation results for the distributed targets, representing precipitation. Two distributed targets are included in 10–$25°$ and 25–$45°$, retrieving the peak levels of -68 and -60 dBm, respectively. The FR and MMSE estimations are almost the same. Although the two targets are accurately detected using both methods, they are overestimated by approximately 7 dB around the targets (0–$10°$ and 45–$60°$). In contrast, the scMMSE estimation is more accurate because the RMSEs of FR, MMSE, and scMMSE for the truth are 7.0, 7.5, and 2.1 dB, respectively. These results indicate that scMMSE is effective for DP-PAWR observations. In the next section, we only consider FR and scMMSE because MMSE without steering vector correction is not effective for point targets and exhibits comparable performance to FR for distributed targets.

B. Effect of Phase Error

In phased-array systems, the effect of amplitude errors, i.e., random errors, on the beam combination efficiency is relatively small [22], and phase errors between antenna elements undermine beamforming [23], [24]. In practical use, it is important to understand the performance of a beamforming method when the
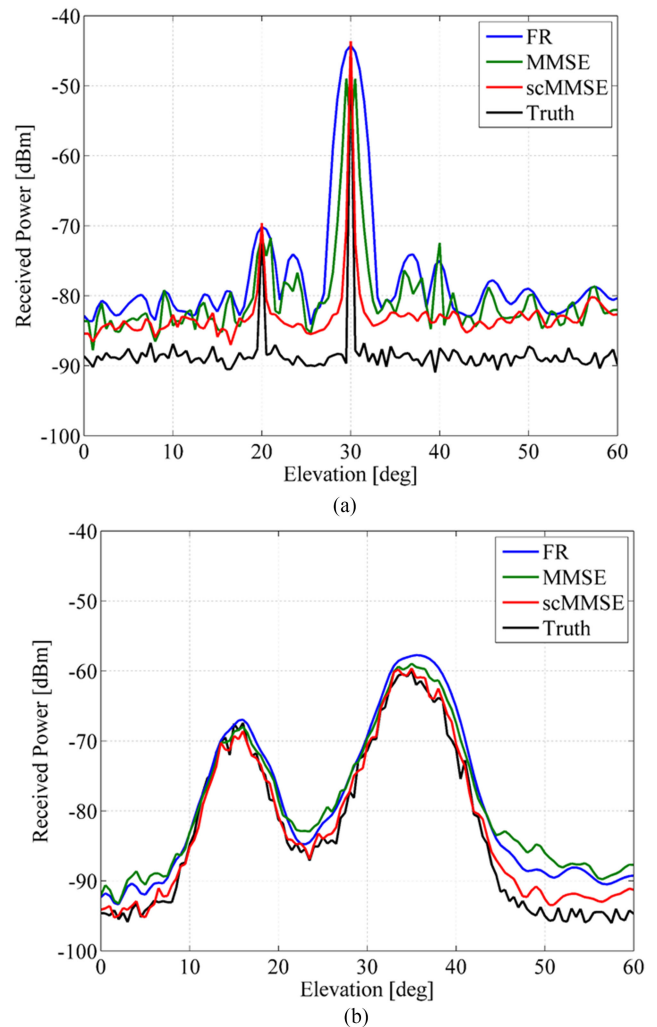

Fig. 3.   Simulation results for (a) point and (b) distributed targets.

phase errors are included in each antenna element. We conducted numerical simulations to analyze the effect of the phase error in terms of subarrays and ground clutter on the polarimetric parameters of the DP-PAWR. Fig. 4 shows the estimation results of the FR and scMMSE for clutter and precipitation present in the observation range for elevation angles ranging from $0°$ to $90°$. The clutter echo (point target) is set at $1°$, and the precipitation echo (distributed target) is set in elevation angles ranging from $10°$ to $50°$. Fig. 4(a-1), (a-2), (a-3), and (a-4) show the estimations of FR, scMMSE, and true values of horizontal radar reflectively factor (Z_{h}), differential reflectivity (Z_{dr}), specific phase difference (K_{dp}), and correlation coefficient (ρ_{hv}), respectively, at the phase error of 0 rad.

In Fig. 4(a-1), FR shows overestimation around clutter at elevation angles of 2–$18°$. At higher elevation angles, 50–$90°$, an overestimation of approximately 18 dB occurs because of the high sidelobes of FR. In contrast, scMMSE suppresses the overestimation of 20 dB around clutter and at elevation angles above $50°$. In Fig. 4(a-2), Z_{dr} obtained using FR is also highly
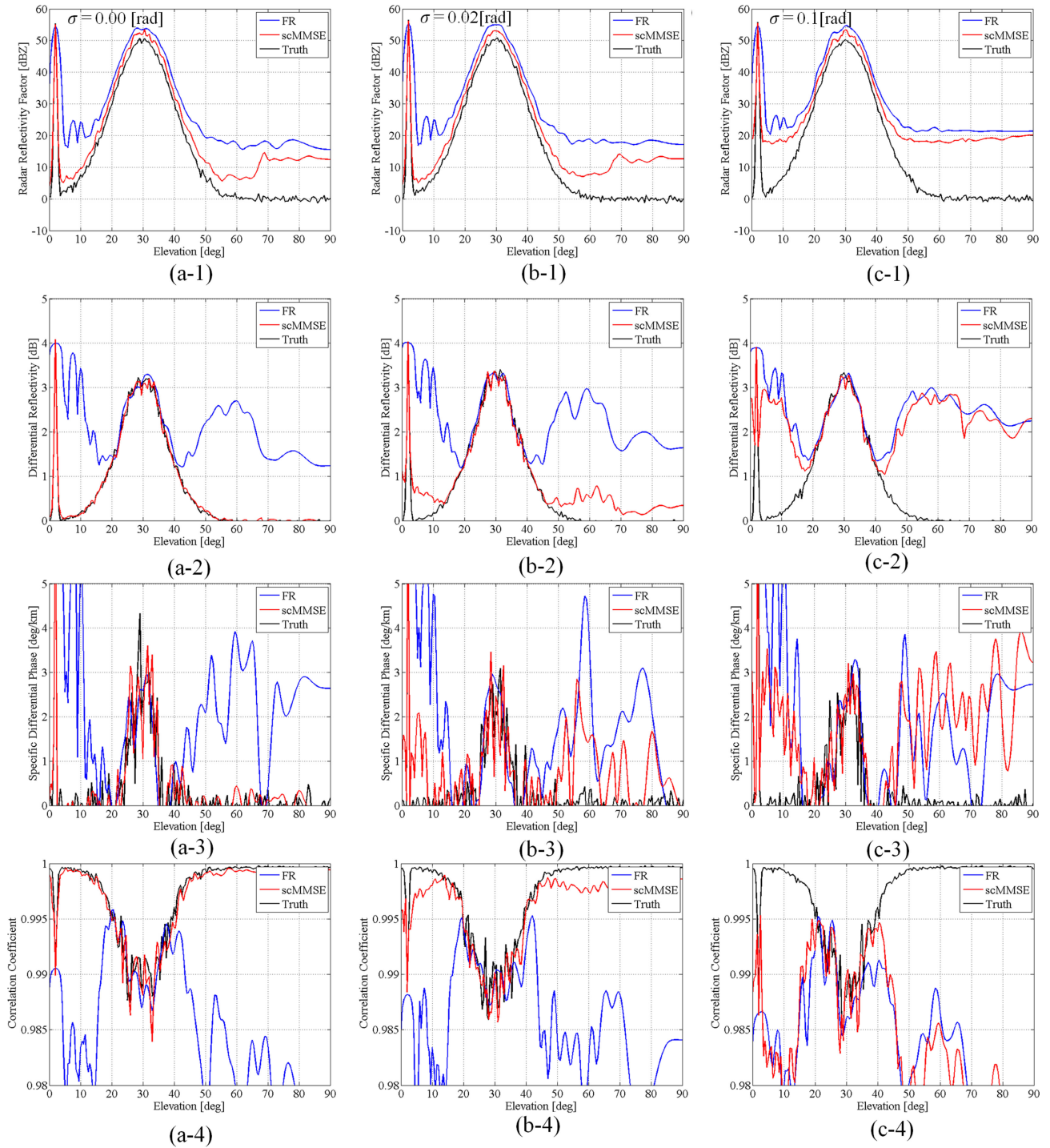
Fig. 4. Estimation results of FR and scMMSE for clutter and precipitation targets in observation range. Labels 1–4 show the estimation results of FR and MMSE for horizontal radar reflectively factor (Z_{h}), differencial reflectivity (Z_{dr}), specific phase difference (K_{dp}), and correlation coefficient (ρ_{hv}), respectively. Labels (a)–(c) indicate phase errors of 0°, 0.02°, and 0.1°, respectively.

overestimated at elevation angles of 2–10° and above 40° for phase errors of 0 rad in the antenna elements. At elevations from 10° to 50°, the precipitations are clearly detected by FR. On the other hand, Z_{dr} obtained using the proposed scMMSE is more accurate at all elevations. Fig. 4(a-3) and (a-4) show that K_{dp} and ρ_{hv} obtained using scMMSE are effective for the clutter and

precipitation echoes. FR accurately estimates K_{dp} and ρ_{hv} in the range of strong radar reflectivity factors at elevation angles of 25–40°.

Fig. 4(b-1)–(b-4) show the estimation results under random phase errors of 0.02 rad. Z_{h} obtained using FR is almost the same as for zero phase error, as shown in Fig. 4(a-1), whereas
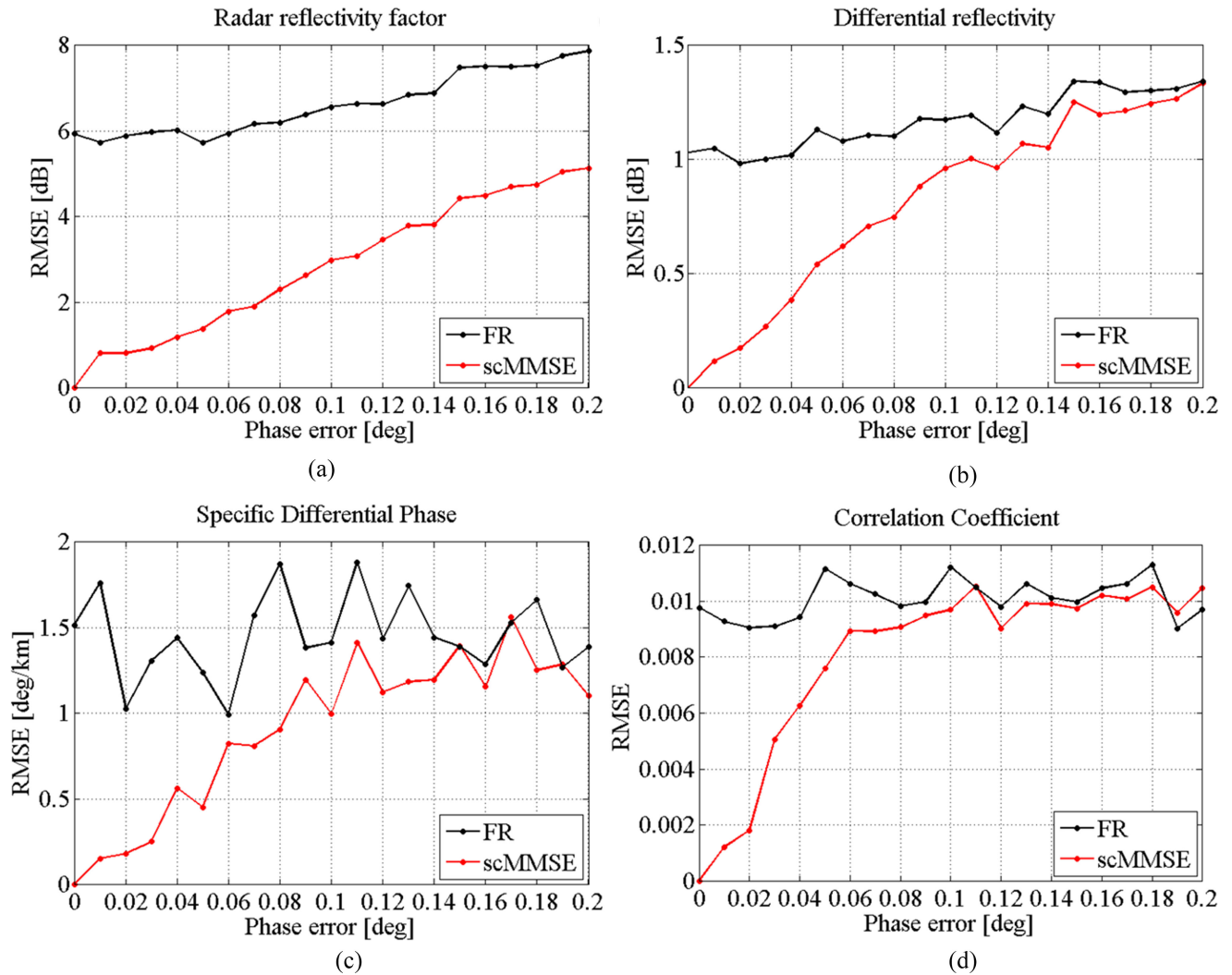
Fig. 5. RMSE of estimation results of FR/scMMSE, and true values for parameters (a) Z_{h}, (b) Z_{dr}, (c) K_{dp}, and (d) ρ_{hv}.

the proposed scMMSE estimates Z_{h} with a slight overestimation of approximately 1 dB at high elevation angles.

In Fig. 4(b-2), scMMSE shows slight overestimation of Z_{dr} of approximately 0.5 dB due to the effect of phase errors. However, overestimations are not fatal errors because they exist outside the target range at elevation angles ranging from 10° to 50°. In case of Z_{dr} obtained using FR, there are no clear differences between Fig. 4(a-2) and (b-2). In Fig. 4(b-3) and (b-4), the values of K_{dp} and ρ_{hv} obtained using scMMSE are accurate for the range where target signals exist.

At a phase error of 0.1 rad, the FR and scMMSE estimations of all parameters have almost the same accuracy as those shown in Fig. 4(c-1)–(c-4), with the results being highly overestimated. Therefore, scMMSE is not effective when the phase error is 0.1 rad, whereas FR seems insensitive to phase errors.

Fig. 5 shows the RMSE of the estimation results of FR and scMMSE, and scMMSE with phase error of 0 rad. Fig. 5(a)–(d) show the RMSEs of Z_{h}, Z_{dr}, K_{dp}, and ρ_{hv} in the range where the target signals exist at elevations of 10–50°. The estimation errors of scMMSE are suppressed below 0.8 dB, 0.12 dB,

0.2 deg/km, and 0.002 for Z_{h}, Z_{dr}, K_{dp}, and ρ_{hv}, respectively, for phase errors below 0.02 rad. With respect to phase error, the estimation accuracy of scMMSE shows gradual degradation, reaching comparable accuracy to FR. These results confirm that FR estimation is insensitive to phase error ranging from 0 to 0.2 rad, and scMMSE is effective and practical in the case of phase errors below 0.02 rad.

IV. EVALUATION OF REAL MEASUREMENT DATA OF DP-PAWR

To apply the proposed beamforming method to real measurement data, we performed phase error correction as described in our previous study [25]. To ensure a phase error below 0.02 rad, the window size of the median filter in section I-D [25] was set to 18. This correction method reduces the characteristic dispersion of the channel output even under intrinsic dispersion in phase. In this study, I/Q data obtained from the DP-PAWR on July 23, 2019 at 12:12:10 (JST), which was a sunny day, were used. The data were obtained in the southeast direction (azimuth of
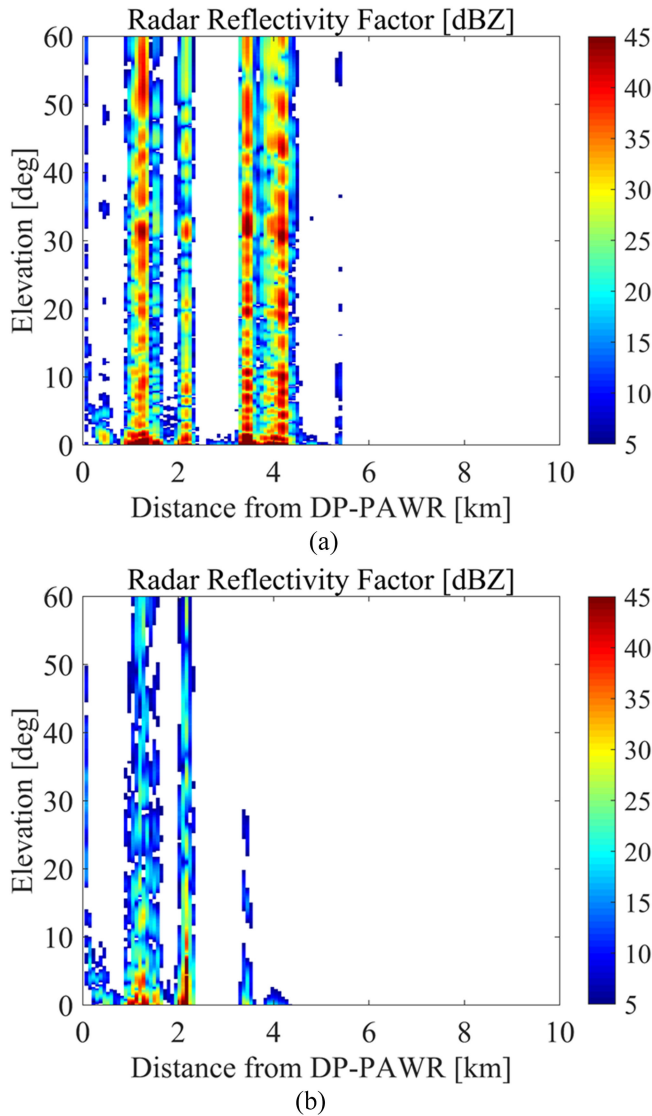
Fig. 6. Range–elevation cross sections of Z_h obtained from (a) FR and (b) scMMSE.

110° from north). In the data, ground clutter was noticeable at the lowest elevation of 0°.

Fig. 6 shows the range–elevation cross sections of Z_h at an elevation of 0–60°. The results in Fig. 6(a) and (b) correspond to FR and scMMSE, respectively. There are strong echoes in the 0–6-km range. In Fig. 6(a), the overestimation of FR is caused at higher elevation angles ranging from 10° to 60°, which are produced by the high sidelobes with the same simulation results as shown in Fig. 4(a-1). For scMMSE, as shown in Fig. 6(b), the scMMSE suppresses clutter echoes of about 30 dB at higher elevation angles even under the strong clutter influence in 0–6 km. Almost all the clutter echoes around the distance of 4 km are eliminated by scMMSE, except for those at approximately 2 km. Although the strong clutter echoes of 45 dBZ at the distances of 1.5 and 2 km are slightly overestimated, the clutter suppression by scMMSE is clearly superior to that by FR. In the future, we need to solve the problem of very strong clutters, which are not enough to suppress echoes, using a combination with other methods such as the Doppler spectrum analysis.

V. CONCLUSION

We developed an adaptive digital beamforming method based on MMSE for application in a newly developed DP-PAWR that has different characteristics than the SP-PAWR. Particularly, the received power of the DP-PAWR differs at each subarray given the different numbers of patch antennas. Hence, steering vector errors occur in the amplitude of the DP-PAWR. Furthermore, we propose an estimation method that optimizes the steering vector for the DP-PAWR and minimizes ground clutter influence. The effectiveness of the proposed MMSE with steering vector correction, scMMSE, was verified and compared with the results of FR by conducting numerical simulations for both point and distributed targets. Additional numerical simulations allow the effect of phase error to be analyzed considering the effects of antenna elements and ground clutter on the polarimetric parameters of the DP-PAWR. The estimation errors of scMMSE are suppressed below 0.8 dB, 0.12 dB, 0.2 deg/km, and 0.002 for Z_h, Z_{dr}, K_{dp}, and ρ_{hv}, respectively, for phase errors below 0.02 rad. Hence, the phase error of subarrays should be kept below 0.02 rad to successfully apply the proposed scMMSE. After phase error correction, we applied FR and scMMSE to real measurement data of the DP-PAWR. Clutter suppression obtained using scMMSE is clearly superior to that obtained using FR. In general, our developed method and results should allow the evaluation of the applicability of adaptive digital beamforming to a phased-array radar system, in which it is difficult to maintain adequate phase and gain accuracies.

Although the proposed method has been applied for clutter data with DP-PAWR, it could not be applied for precipitation data in this article. This is because we do not possess the precipitation data because we have not yet had the opportunity to perform an investigation in that regard. Therefore, in this study, the observation accuracy of the dual polarization radar variables using the proposed method were evaluated using numerical simulations. Although the results of the simulations are sufficient to indicate the effectiveness of the proposed method, we plan to obtain actual weather data in the future and thereafter apply the proposed method.

REFERENCES

[1] D. S. Zrnic *et al.*, "Agile-beam phased array radar for weather observations," *Bull. Amer. Meteorol. Soc.*, vol. 88, no. 11, pp. 1753–1766, Nov. 2007.

[2] P. L. Heinselman, D. L. Priegnitz, K. L. Manross, T. M. Smith, and R. W. Adams, "Rapid sampling of severe storms by the national weather radar testbed phased array radar," *Weather Forecast.*, vol. 23, no. 5, pp. 808–824, Oct. 2008.

[3] K. A. Orzel and S. J. Frasier, "Weather observation by an electronically scanned dual-polarization phase-tilt radar," *IEEE Trans. Geosci. Remote Sens.*, vol. 56, no. 5, pp. 2722–2734, May 2018.

[4] W. Heberling and S. J. Frasier, "Evaluation of phased-array weather-radar polarimetry at X-band," in *Proc. IEEE Radar Conf.*, Oklahoma City, OK, USA, 2018, pp. 851–855.

[5] C. Fulton *et al.*, "Cylindrical polarimetric phased array radar: Beamforming and calibration for weather applications," *IEEE Trans. Geosci. Remote Sens.*, vol. 55, no. 5, pp. 2827–2841, May 2017.

[6] M. M. French, H. B. Bluestein, I. PopStefanija, C. A. Baldi, and R. T. Bluth, "Reexamining the vertical development of tornadic vortex signature in supercells," *Monthly Weather Rev.*, vol. 141, no. 12, pp. 4576–4601, Dec. 2013.

[7] M. M. French, H. B. Bluestein, I. PopStefanija, C. A. Baldi, and R. T. Bluth, "Mobile, phased-array, doppler radar observations of tornadoes at X band," *Monthly Weather Rev.*, vol. 142, no. 3, pp. 1010–1036, Mar. 2014.

[8] B. Isom *et al.*, "The atmospheric imaging radar: Simultaneous volumetric observations using a phased array weather radar," *J. Atmos. Ocean. Technol.*, vol. 30, no. 4, pp. 655–675, Apr. 2013.

[9] C. Wu, L. Liu, X. Liu, G. Li, and C. Chen, "Advances in Chinese dual-polarization and phased-array weather radars: Observational analysis of a supercell in southern China," *J. Atmos. Ocean. Technol.*, vol. 35, no. 9, pp. 1785–1806, Sep. 2018.

[10] F. Mizutani, *et al.*, "Fast-scanning phased array weather radar with angular imaging technique," *IEEE Trans. Geosci. Remote Sens.*, vol. 56, no. 5, pp. 2664–2673, May 2018.

[11] H. Kikuchi, T. Ushio, F. Mizutani, and M. Wada, "Improving the accuracy of rain rate estimates using X-band phased-array weather radar network," *IEEE Trans. Geosci. Remote Sens.*, vol. 56, no. 12, pp. 6986–6994, Dec. 2018.

[12] T. Adachi, K. Kusunoki, S. Yoshida, K. Arai, and T. Ushio, "High-speed volumetric observation of a wet microburst using X-band phased array weather radar in Japan," *Monthly Weather Rev.*, vol. 144, no. 10, pp. 3749–3765, Oct. 2016.

[13] V. N. Bringi and V. Chandrasekar, *Polarimetric Doppler Weather Radar: Principles and Applications*. Cambridge, UK: Cambridge Univ. Press, 2001.

[14] T. A. Seliga and V. N. Bringi, "Potential use of radar differential reflectivity measurements at orthogonal polarizations for measuring precipitation," *J. Appl. Meteorol.*, vol. 15, no. 1, pp. 69–76, Jan. 1976.

[15] G. Scarchilli, E. Gorgucci, V. Chandrasekar, and T. A. Seliga, "Rainfall estimation using polarimetric techniques at C-band frequencies," *J. Appl. Meteorol.*, vol. 32, no. 6, pp. 1150–1160, Jun. 1993.

[16] A. Ryzhkov, D. Zrnić, and D. Atlas, "Polarimetrically tuned R (Z) relations and comparison of radar rainfall methods," *J. Appl. Meteorol.*, vol. 36, no. 4, pp. 340–349, Apr. 1997.

[17] A. V. Ryzhkov, T. J. Schuur, D. W. Burgess, P. L. Heinselman, S. E. Giangrande, and D. S. Zrnić, "The joint polarization experiment: Polarimetric rainfall measurements and hydrometeor classification," *Bull. Amer. Meteorol. Soc.*, vol. 86, no. 6, pp. 809–824, Jun. 2005.

[18] E. Yoshikawa *et al.*, "MMSE beam forming on fast-scanning phased array weather radar," *IEEE Trans. Geosci. Remote Sens.*, vol. 51, no. 5, pp. 3077–3088, May 2013.

[19] S. D. Blunt and K. Gerlach, "Adaptive pulse compression via MMSE estimation," *IEEE Trans. Aerosp. Electron. Syst.*, vol. 42, no. 2, pp. 572–584, Apr. 2006.

[20] S. D. Blunt and T. Higgins, "Achieving real-time efficiency for adaptive radar pulse compression," in *Proc. IEEE Radar Conf.*, Waltham, MA, USA, 2007, pp. 116–121.

[21] T. Higgins, S. D. Blunt, and K. Gerlach, "Gain-constrained adaptive pulse compression via an MVDR framework," in *Proc. IEEE Radar Conf .*, Pasadena, CA, USA, 2009, pp. 1–6.

[22] T. Y. Fan, "The effect of amplitude (power) variations on beam combining efficiency for phased arrays," *IEEE J. Sel. Topics Quantum Electron.*, vol. 15, no. 2, pp. 291–293, Mar./Apr. 2009.

[23] C. T. Lancée, J. M. Vissers, S. Mientki, C. M. Ligtvoet, and N. Bom, "Influence of phase errors on beam-steered phased arrays," *Ultrasonics*, vol. 25, no. 3, pp. 154–159, May 1987.

[24] H. S. C. Wang, "Performance of phased-array antennas with mechanical errors," *IEEE Trans. Aerosp. Electron. Syst.*, vol. 28, no. 2, pp. 535–545, Apr. 1992.

[25] H. Kikuchi, E. Yoshikawa, T. Ushio, F. Mizutani, and M. Wada, "Application of adaptive digital beamforming to Osaka University phased array weather radar," *IEEE Trans. Geosci. Remote Sens.*, vol. 55, no. 7, pp. 3875–3884, Jul. 2017.

[26] A. V. Ryzhkov, S. E. Giangrande, V. M. Melnikov, and T. J. Schuur, "Calibration issues of dual-polarization radar measurements," *J. Atmos. Ocean. Technol.*, vol. 22, no. 8, pp. 1138–1155, Aug. 2005.

Hiroshi Kikuchi (Member, IEEE) received the B.S. degree from the Department of Engineering, Doshisha University, Kyoto, Japan, in 2008, and the M.S. and Ph.D. degrees from the Division of Electrical, Electronic, and Information Engineering, Osaka University, Suita, Japan, in 2010 and 2013, respectively, all in engineering.

In 2013, he joined the Division of Electrical, Electric and Information Engineering, Osaka University as a Specially Appointed Researcher. In 2017, he was a Research Assistant Professor with Tokyo Metropolitan University. In 2018, he joined the University of Electro-Communications, Tokyo, Japan, where he is currently an Assistant Professor. His research specialties are the remote sensing for an atmospheric electricity with space-borne platforms, and the weather radar remote sensing and a development of the radar system.

Eiichi Yoshikawa (Member, IEEE) was born in Osaka, Japan, in 1981. He received the B.S. degree in aerospace engineering from Osaka Prefecture University, Osaka, Japan, in 2005, and the M.S. and Ph.D. degrees in engineering from Osaka University, Osaka, Japan, in 2008 and 2010, respectively.

In 2011, he was with Osaka University and Colorado State University, as a Postdoctoral Researcher. He is currently with the Japan Aerospace Exploration Agency (JAXA), Tokyo, Japan. His research specialties are radar-based remote sensing, signal processing, and atmospheric science.

Tomoo Ushio (Member, IEEE) received the B.S., M.S., and Ph.D. degrees in electrical engineering from Osaka University, Suita, Japan, in 1993, 1995, and 1998, respectively.

From 1998 to 2000, he was with the Global Hydrology and Climate Center, Huntsville, AL, USA, as a Postdoctoral Researcher. In 2000, he joined the Department of Aerospace Engineering, Osaka Prefecture University. In 2006, he was with the Department of Electrical, Electronic and Information Engineering, Osaka University, as an Associate Professor. Since 2019, he has been a Professor with Osaka University. His research specialties are radar-based remote sensing, passive and active remote sensing of atmosphere from space borne platforms, and atmospheric electricity.

Yasuhide Hobara received the B.S., M.S., and Ph.D. degrees in electrical engineering from The University of Electro-Communications (UEC), Tokyo, Japan, in 1991, 1994, and 1997, respectively.

Following his graduation from the UEC, he worked with the Institute of Applied Physics (Russia), Earth Observation Research Center, JAXA, Laboratoire de Physique et Chimie de l'Environnement et de l'fEespace, CNRS (France), Swedish Institute of Space Physics (Sweden), The University of Sheffield (U.K.), and Tsuyama National College of Technology (Japan). He joined the Department of Computer and Network Engineering, Engineering, Graduate School of Informatics and Engineering, UEC, in 2009, where he is currently a Professor. Terrestrial and space electromagnetic environment are his main fields of research including space plasma science, atmospheric electricity, and seismo-electromagnetics.